

EvMAPPER: High Altitude Orthomapping with Event Cameras

Fernando Cladera, Kenneth Chaney,
M. Ani Hsieh, Camillo J. Taylor, and Vijay Kumar

Abstract—Traditionally, unmanned aerial vehicles (UAVs) rely on CMOS-based cameras to collect images about the world below. One of the most successful applications of UAVs is to generate orthomosaics or orthomaps, in which a series of images are integrated together to develop a larger map. However, the use of CMOS-based cameras with global or rolling shutters mean that orthomaps are vulnerable to challenging light conditions, motion blur, and high-speed motion of independently moving objects under the camera. Event cameras are less sensitive to these issues, as their pixels are able to trigger asynchronously on brightness changes. This work introduces the first orthomosaic approach using event cameras. In contrast to existing methods relying only on CMOS cameras, our approach enables map generation even in challenging light conditions, including direct sunlight and after sunset.

The source code for EvMAPPER, the high-altitude hardware, and the dataset collected in this paper are available open source¹.

I. INTRODUCTION

High-altitude photography has proven useful for surveillance, mapping and inspection applications. High-vantage points can provide information that is not easily accessible by ground imaging. Additionally, high-altitude photography offers superior ground resolution distance (GRD) compared to satellite imagery. This advantage is due to lower flight altitude, the limitations imposed by the Rayleigh criterion limit [1], and reduced effects of atmospheric conditions [2].

High-altitude images are usually integrated together into orthomosaics by projecting the images into a planar map. Orthomosaics are generated with proven computer vision techniques, such as structure from motion (SFM) and mesh reconstructions. There are multiple commercial-off-the-shelf (COTS) software packages for creating orthomosaics, such as Pix4D [3] and OpenDroneMap (ODM) [4]. The orthomosaic's quality directly depends on the quality of the input images. Generating orthomosaics is an offline process that is prone to failures if the data is not properly conditioned. For example, blurry images may lead to fewer features and hinder the feature matching process. Similarly, low overlap between images, strong winds, or vibrations can also lead to failures [5].

Some of the issues encountered during orthomosaic creation stem from the limitations of the sensors employed.

All authors are with GRASP Laboratory, University of Pennsylvania. Corresponding author: fclad@seas.upenn.edu.

We gratefully acknowledge the support of ARL DCIST CRA W911NF-17-2-0181, NIFA grant 2022-67021-36856, the IoT4Ag Engineering Research Center funded by the National Science Foundation (NSF) under NSF Cooperative Agreement Number EEC-1941529, and NVIDIA.

¹<https://evmapper.fcladera.com>



Fig. 1. Top: The Falcon 4 aerial platform used for high-altitude experiments. The sensor stack, equipped with an IMU, a range sensor, an RGB camera, and an event camera, was mounted at the front. Bottom left: artifacts of CMOS-based cameras in high-altitude photography: the sidewalk is washed out due to high brightness. Bottom right: reconstructed frame with event cameras displaying higher level of detail in challenging light conditions.

CMOS-based cameras are susceptible to motion blur due to wind or unmanned aerial vehicle (UAV) vibration, particularly when long exposures are used. Their limited dynamic range makes it difficult to capture regions with both high brightness and shadows. Fast movements under the camera, resulting from high flight speeds, can lead to failed feature matches for SFM. Finally, rolling-shutter CMOS-based cameras are susceptible to distortion due to the linear readout of pixels. Some of the examples of these issues are observed in Fig. 1. There are strengths to CMOS-based cameras and to overcome the above limitations we seek methods to replace and/or augment existing CMOS-based camera data.

Event cameras are increasingly used in robotics to overcome the limitations of CMOS-based cameras, thanks to their superior dynamic range, higher temporal resolution, and reduced motion blur. Recently, event cameras have seen a significant increase in resolution, nearing the 1 Megapixel mark. This resolution increase makes event cameras useful for applications where high detail is required. While some

works have used event cameras for high-altitude HDR [6] imaging or low-light navigation [7], no prior work has explored the use of event cameras for high-resolution orthomosaics. We believe that event cameras can be leveraged to overcome the limitations of traditional imaging sensors in various robotics applications, particularly given the recent success of high-altitude imaging using UAVs. However, to employ event cameras for use in orthomosaic mapping, we require a sensor stack which can collect time synchronized data to allow event fusion. Additionally, we need processing methods to convert the collected event data into a format compatible with existing open source orthomosaic mapping tools.

Our contributions are:

- The development of a hardware and software architecture to capture synchronized high-resolution events, RGB images, IMU measurements, and range measurements.
- A method to integrate the event camera data into off-the-shelf orthomosaic generation tools, and benchmark the results against RGB reconstructions.
- An open-source high-altitude event camera dataset, comprising synchronized data of our high-altitude UAV flying in challenging light conditions and at high speed.

Our contributions demonstrate that event-camera orthomapping is a promising direction of research, and our dataset provides vital baselines for future researchers in the field.

II. RELATED WORK

The most relevant research related to our work can either be classified as using event cameras to increase the dynamic range of RGB cameras or leveraging them for event reconstruction. We briefly summarized this existing work.

Event cameras feature a high dynamic range as each pixel in the sensor can trigger independently of the other ones. Some works have leveraged event cameras to increase the dynamic range of CMOS-based cameras. In [8], the authors pioneered the use of mixed representations, fusing image frames and events. In [9], the authors used event cameras to deblur and enhance a video stream before upsampling. In [10], the authors proposed a network architecture using deformable convolutions and LSTM to enhance the dynamic range in static images. The authors used a similar set of sensors to the ones used in this work mounted on a beam-splitter setup. More recently, Li et al. [6] recognized that event cameras can be used to enhance the dynamic range of aerial images. The authors propose a gradient-enhanced high dynamic range (HDR) reconstruction network coupled with an event-based dynamic range enhancement network. While these existing works highlight the advantages of event cameras for aerial imaging, they do not address the integration of the sensor for mapping.

Multiple works have focused on reconstruction of brightness frames from event data. Reconstructed images could be used to apply mature computer vision algorithms [11]. We apply this approach in our work, leveraging existing tools for orthomapping. Besides higher dynamic range, reconstructed

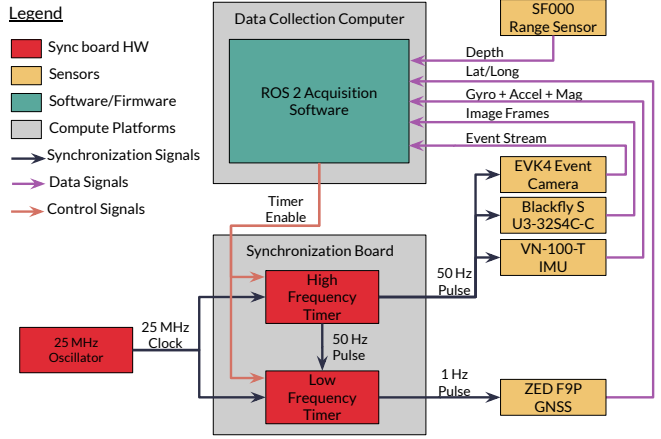


Fig. 2. System architecture for data acquisition. The synchronization board generates pulse signals that are used to trigger (Blackfly S) or timestamp sensors (event camera, IMU, GNSS). Data is collected on an onboard computer running ROS 2, and synchronization is performed after the fact. The single-point LiDAR distance sensor is the only sensor that is not hardware synchronized.

frames also have a higher temporal resolution, allowing for high-speed video reconstruction [12]. Event reconstruction can be performed using filter-based methods [8], pixel-wise integration [13], [14], [15], or learning methods. E2VID [12], [16] proposed a UNet-like architecture to synthesize networks from events, with outstanding results. As we are interested in textures of the environment, we rely on event reconstruction as part of our pipeline.

III. METHODS

To address the problem of using event cameras for orthomosaic mapping, we need time-synchronized sensor data. We also need to preprocess this data to adapt it to existing orthomosaic mapping frameworks.

A. UAV and Data Acquisition Hardware

1) *Time Synchronization*: Time synchronization is essential for multi-sensor datasets including event cameras, due to the high resolution of the sensors [17], [18]. In this work, time synchronization was achieved using physical synchronization signals between the different sensors, as shown in Fig. 2.

A synchronization board based on the STM32L011 microcontroller generates signals using two synchronized timers at 50 Hz and 1 Hz. The 50 Hz signal is used to trigger frame captures on the RGB camera. Additionally, the event camera and the IMU use this signal to timestamp their measurements. Specifically, on the event camera, every time a signal is received, the local sensor timestamp is recorded and transmitted to the computer as part of the event stream. In addition, each IMU message includes the time elapsed between the current measurement and the last synchronization signal. A similar timestamping mechanism is used for the Global navigation satellite system (GNSS), recording the GNSS timestamp when a synchronization signal is received.

An important problem we address is matching the first synchronization pulse across sensors. To generate an unequivocal *start* signal for all the sensors, we created a

Sequence	Duration [s]	Area	Time of the day	Height [m]	Speed [m/s]	Bias on/off	Overlap [%]	Illumination
F1.D.1	514	A	Noon	40	3	0/0	82%	Cloudy
F1.D.2	507	A	Noon	40	3	50/50	82%	Cloudy
F2.D.1	615	A	Afternoon	40	3	50/50	64%	Sunny
F2.D.2	614	B	Afternoon	40	3	100/100	64%	Sunny
F2.D.3	528	A	Evening	40	3	50/50	64%	Sunny
F2.D.4	541	A	Evening	40	3	0/0	64%	Sunny
F2.N.1	555	A	Sunset	40	3	0/0	64%	-
F2.N.2	554	A	Dusk	40	3	50/50	64%	-
F2.N.3	541	A	Night	40	3	100/100	64%	-
F3.D.1	1282	A	Afternoon	35	3	0/0	80% (cross-hatch)	Cloudy
F3.D.2	671	A	Afternoon	40	3	0/0	82%	Cloudy
F3.D.3	558	A	Evening	35	6	0/0	80%	Cloudy
F3.D.4	489	A	Evening	35	9	0/0	80%	Cloudy
F3.N.1	832	A	Sunset	35	3	0/0	80%	-
F3.N.1	853	A	Dusk	35	3	0/0	80%	-

TABLE I

DATA SEQUENCES FOR THE HIGH-ALTITUDE EVENT CAMERA DATASET, SHOWCASING DIFFERENT LIGHT CONDITIONS, FLIGHT PATTERNS, AND BIASES.

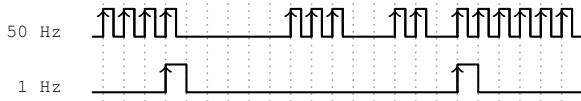


Fig. 3. Time synchronization pattern inserted in the synchronization signal. The *silence gaps* in the signal are predefined, enabling to identify the beginning of the timing sequence for all the sensors.

temporal pattern in the synchronization signal upon receipt of the *timer_enable* command by the data collection computer. Data synchronization can be performed after the fact by analyzing the different timestamps of the messages. An example of the temporal pattern can be observed in Fig. 3.

2) *Hardware description*: Collecting data for orthomosaic mapping requires building a hardware sensor suite that satisfies the payload capabilities of a UAV, including an event camera and RGB camera. As such, we perform experiments with the Falcon 4 platform [19], fitted with a data collection computer with an AMD Ryzen 9 7940HS processor, 32 GB of RAM, and 1 TB SSD. The flight controller is an ARKV6X, capable of flying pre-defined GPS waypoint missions.

The UAV is fitted with the following sensors:

- **FLIR Blackfly S BFS-U3-32S4C-C**: RGB camera, with an IMX252 sensor (2048x1536). The camera is fitted with a Kowa LM5JCM, and captures images at 50 Hz. The field of view (FoV) of the camera is $71^\circ \times 56^\circ$. The exposure time for this sensor is adjusted automatically between 5 ms and 15 ms, using the exposure controller from *flir_camera_driver* [20].
- **SilkyEVCamHD**: IMX636-based event camera, fitted with a LM5JCM lens. We use event camera biases to configure the sensitivity of the sensor to different light conditions. For our experiments, we set all the biases to zero, except *bias_diff_on* and *bias_diff_off* which were set to 0, 50 and 100 for different sequences. The FoV of the camera is $64^\circ \times 39^\circ$. In our previous work [17] we observed that using an event rate controller (ERC) negatively impacts the quality of the events. Therefore, we conducted our data collection without employing an ERC.
- **VN-100-T IMU**: 9-DOF temperature compensated

IMU, running at 400 Hz. The IMU provides an attitude estimation, compensated acceleration, compensated angular rates, and pressure measurements.

- **SF000/B range sensor**: mounted between the two cameras, it provides a single-point depth estimate of the image under the cameras. This sensor captures data at ≈ 60 Hz. The range sensor is the only sensor in our stack that lacks hardware synchronization capability. This is not a major limitation in this work, as we only use the sensor to determine an adequate altitude to start and stop processing data, as described in Sec. III-C.
- **ZED-F9P GNSS**: runs at 5 Hz in multi-constellation configuration. A TOP106 multi-band L1/L2 antenna is used to maximize satellite count and minimize interference from the UAV onboard computer.

All these sensors with exception of the GNSS module are fitted in a rigid carbon fiber plate, and attached to the UAV using vibration-absorbing foam pads. Dampening is critical to reduce high-frequency vibrations from the motors of the UAV, which may generate a significant number of events. Fig. 1 shows a picture of the platform with the sensor stack, and Fig. 2 presents an overview of the system architecture.

B. Data Collection Procedure

We collected 15 sequences with our high altitude UAV at the Pennovation campus in Philadelphia, PA, USA. This location showcases a semi-urban environment, with buildings and green areas with grass and trees. The flight area is ap-

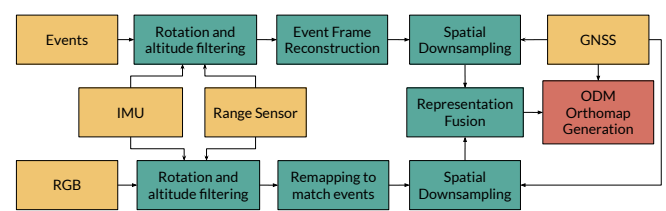


Fig. 4. EvMAPPER data preprocessing pipeline. Events and RGB images are collected when the UAV is not performing aggressive rotations. Events are reconstructed into frames, and RGB images are remapped to match the event frames. The resulting representations are fed into an off-the-shelf orthomap generation tool.



Fig. 5. Ground truth reconstruction using F3.D.1 and F3.D.2 sequences. Left: Orthophoto. Right: Point cloud.

proximately 11700 m². Flights were performed at an altitude of 35 m or 40 m above ground level (AGL), using pre-defined lawnmower pattern missions. The details about the sequences are in Tab. I. The speed of the UAV varies from 3 m/s to 9 m/s. Areas A and B correspond to different regions of the campus. The bias setting refers to the event camera configuration described in Sec. III-A.2. Overlap represents the approximate *image overlap* between two parallel flight tracks in the waypoint mission. Finally, the illumination conditions are varied to have enough diversity in the event camera stream.

Sequences are synchronized following the approach described in Sec. III-A.1 and the resulting synchronized files are saved both in MCAP [21] and HDF [22] formats. Camera and IMU calibrations are obtained using Kalibr [23]. To calibrate the event and RGB cameras, events are reconstructed using `simple_image_recon` [14].

C. Data Preprocessing & Orthomosaic Mapping

To ensure the data collected fits within existing orthomosaicing frameworks, we require data preprocessing methods (Fig. 4). This includes filtering, reconstructing the events into frame representations, and downsampling and fusion of the RGB and event representations. Once data is properly prepared, orthomosaic mapping is performed.

High altitude UAVs are affected by vibrations due to their motors and also wind gusts. These vibrations generate motion blur in the RGB images, as well as an increased number of events. In the context of high-altitude imaging, rotational vibrations have the largest impact in the quality of the image. Therefore, the first stage in EvMAPPER is to perform rotation filtering of the events and images using the IMU. This filtering skips data when the UAV is performing an aggressive rotation, *e.g.*, when the UAV is accelerating or stopping at a waypoint. A threshold is used to eliminate values when the norm of the angular velocity is above 0.4 rad/s. Similarly, we want to avoid using data from low-altitude settings when the UAV is taking off or landing. We filter out data when the UAV is below 20 m AGL.

To reconstruct frames from events we leverage E2VID [12]. Reconstructions are performed using 5 ms event windows. The resulting images are monochromatic, with higher dynamic range than the RGB counterparts, yet lacking in low-frequency texture information.

Orthomosaic reconstructions require adequate spacing between frames: too much overlap increases the computational cost of the reconstruction, whereas too little can affect the matching process. The lateral overlap of the images is defined by the mission flight pattern. The longitudinal overlapping is defined by sub-sampling images and events. We use the GNSS for this task, to generate a single image every 2 m.

The representation fusion uses synchronized RGB frames and the event representation to generate a new image. This approach is similar to pansharpening, in which a pair of multispectral and panchromatic images are fused [24]. We selected the Brovey, ESRI, and mean pansharpening approaches to generate the fused representations and evaluate their results in the generated orthomap. RGB images are remapped to the event frame reconstruction before processing, using the calibrations obtained in Sec. III-B.

Finally, the input for the orthomap generation is a set of images and Universal Transverse Mercator (UTM) coordinates which can be obtained from GNSS. The orthomap generation approaches uses the off-the-shelf reconstruction software ODM [4]. A resolution of 1 cm/px was chosen for the orthomosaic generation, with an octree depth of 13, and a minimum number of features of 12000.

IV. RESULTS

A. Evaluation Approach

We generate a ground truth reconstruction using a combination of RGB images from F3.D.1 and F3.D.2 sequences, without performing any modifications to the images. This reconstruction corresponds to the highest quality one available in the dataset: both missions are flown in benign light conditions (cloudy evenings), encompassing a larger area than other flights. In addition, F3.D.1 flight

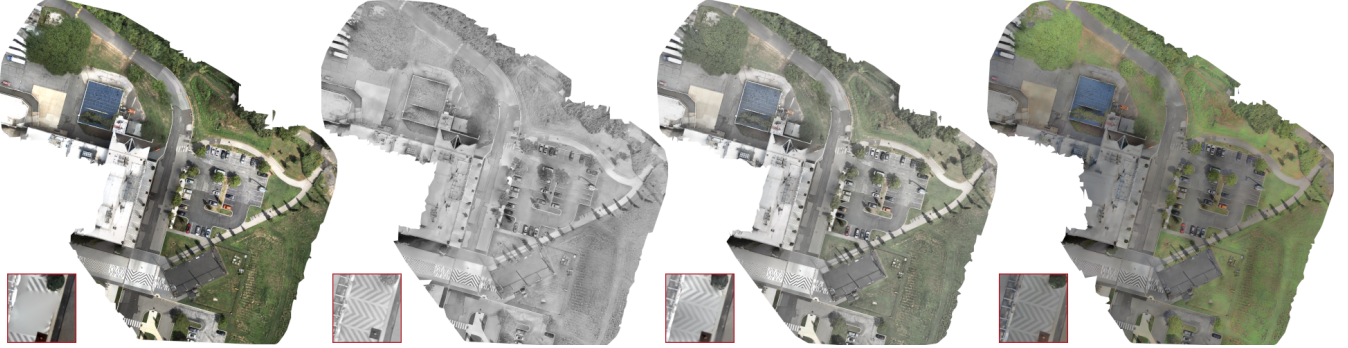


Fig. 6. Resulting reconstructions for the F1.D.1 sequence for cropped RGB, events only, mean fusion and Brovey fusion. The detail (bottom left rectangle) shows the sidewalk reconstruction, an area of high dynamic range. We observe how the RGB reconstruction fails for this particular sequence, whereas the events and fusions are able to display this area correctly.

Sequence	Type	PSNR Color [dB]	PSNR Gray [dB]	SSIM [%]	Non-zero pixels [M]
F1.D.1	RGB Cropped	11.01	10.88	0.54	826.58
F1.D.1	Events Only	9.41	9.39	0.49	953.39
F1.D.1	Mean Fusion	9.87	9.77	0.50	959.39
F1.D.1	ESRI Fusion	9.38	9.26	0.48	953.54
F1.D.1	Brovey Fusion	9.99	9.87	0.51	953.73
F3.N.1	RGB Cropped	12.47	12.41	0.63	692.33
F3.N.1	Events Only	10.52	10.68	0.59	645.12
F3.N.1	Mean Fusion	12.08	12.13	0.65	692.09
F3.N.1	ESRI Fusion	9.64	9.69	0.53	844.95
F3.N.1	Brovey Fusion	10.55	10.46	0.55	844.53
F3.N.2	RGB Cropped	8.05	7.92	0.36	723.62
F3.N.2	Mean Fusion	9.26	9.12	0.48	1022.84

TABLE II

RESULTS ON DATA SEQUENCES FOR HIGH DYNAMIC RANGE (F1.D.1), AND LOW-LIGHT CONDITIONS (F3.N.1 AND F3.N.2).

mission is longer because the UAV flew a cross-hatch pattern, reducing the probability of non-matched images. The ground truth ortophoto and point cloud can be observed in Fig. 5.

We align the test image with the ground truth reconstruction using manual feature matching and homography transformations, using five reference points. We then compute the peak signal-to-noise ratio (PSNR) and structural similarity index (SSIM) metrics between the two images. As the reconstruction may succeed without including the whole set of images, we also report the total number of non-zero pixels. We consider that a reconstruction failed when the reference points for the homography cannot be found, or when ODM fails to generate the orthomosaic.

B. Results and Discussion

The results are in Table II. *RGB cropped* corresponds to the RGB image remapped to the same size as the event image. *Events only* is the reconstruction of the events without fusion with RGB. For reference, a completely black image would have a PSNR of 7.18 dB, whereas a completely white image would have a PSNR of 6.05 dB.

1) *High-brightness conditions*: The sequence F1.D.1 is a high-brightness sequence as it was recorded at noon on a sunny day. We can observe in this sequence that the RGB reconstruction matches the ground truth quite well, achieving the highest PSNR and SSIM. There are, however, some areas of the image that are better reconstructed using events, such as the detail displayed in Fig. 6. Fused and event

representations are able to capture the detail in the sidewalk next to the building, as well as in areas in the shadows.

Among our reconstructions, we observe that mean and Brovey fusion outperform the vanilla event reconstruction. This shows how fusing events with RGB can provide a better reconstruction than using events alone.

2) *Low-light conditions*: We can observe that the proposed method performs well on low-light conditions, as shown by the results in F3.N.1 and particularly F3.N.2. For F3.N.1, the RGB reconstruction still performs slightly better for PSNR, but the SSIM is better for the mean fusion. As this sequence is recorded at sunset, there is still enough light for the RGB sensor to capture the scene. On the other hand, the fusion methods performed better for F3.N.2. It is worth noting that in this sequence the mean fusion was the only method that was able to generate results besides the RGB cropped image. The other methods (ESRI, events only, and Brovey) failed to produce an orthomosaic. We observed this failure mode for numerous reconstructions with low-light conditions, suggesting that mean fusion is a more resilient method compared to other approaches.

Qualitative results can be seen in Fig. 7. We observe that areas with artificial illumination reconstruct well in the RGB images, but the rest of the image is quite dark. On the other hand, the mean fusion method is able to increase the overall brightness of the image, improving the level of detail in parking lots and sidewalks. However, the fusion method increases the overall level of noise in the image, producing

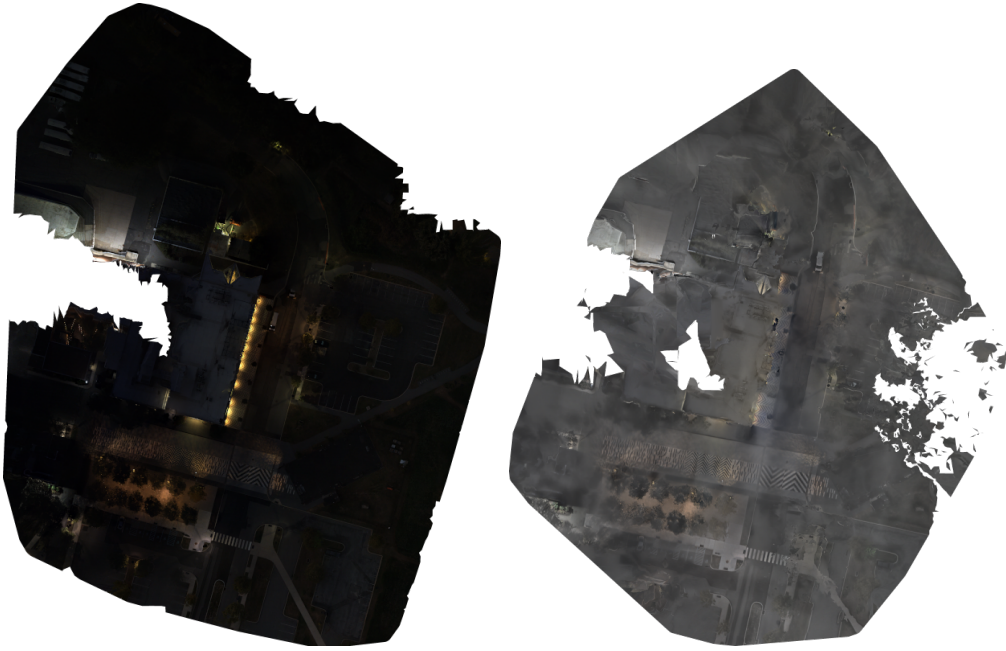


Fig. 7. Orthomap reconstruction results for the F3.N.2 sequence. Left: RGB reconstruction. Right: mean fusion. We observe that the RGB reconstruction has multiple dark areas, while the mean fusion reconstruction increases the overall brightness. Some matching artifacts can be observed in the event reconstruction.

artifacts in the reconstruction.

It was, however, surprising to us that the RGB camera performed well in these very low light situations. This behavior can be explained thanks to the high quantum efficiency of the sensor used (60% at 525nm), and the maximum exposure time of 15 ms.

In our results, we observe that frames synthesized from events are able to overcome the limitations of RGB images given their high dynamic range. Nevertheless, pure event representations struggle with high texture complexities such as grassy areas. We believe this is due to the limitations of the sensor, which generates a significant number of events that may saturate its bandwidth.

V. CONCLUSION

In this work, we presented a method for high-altitude orthomapping using event cameras. To our knowledge, this is the first work that leverages the characteristics of event cameras to overcome the issues of CMOS-based sensors in this setting. We demonstrated that our method enables the creation of orthomosaics in low-light conditions, as well as qualitative improvements in high dynamic range areas.

Given the success of this work, there are exciting possibilities for future work. For example, the experiment area for this paper offered a limited amount of high dynamic range scenarios, and thus the overall PSNR and SSIM metrics performed better than event-based reconstructions. We expect event based orthomosaic mapping to perform better in more challenging scenarios, such as forests at noon. Furthermore, in this work, we leveraged traditional image processing pipelines to produce the orthomosaics, which relies on FLANN features for matching [25]. How-

ever, feature tracking in the event space may provide more resilient tracking, particularly in low-light conditions [26], [27]. Additionally, although we relied on GNSS priors to generate the reconstruction, there are promising future directions using event-based SLAM approaches for orthomapping reconstruction, such as the ones proposed by [28]. Finally, we used traditional methods for pansharpening. Consequently, we observed that the noise in the fused images was higher than the base RGB. Generative methods have outperformed traditional methods in satellite imaging and one possibility is training these generative methods on event data to yield sharper reconstructions.

ACKNOWLEDGMENTS

The authors would like to thank Alex Zhou and Jeremy Wang for their help maintaining the platforms and manufacturing the hardware components of the UAV, and Benedict Onyekwe for his help routing the synchronization board. We would like to acknowledge the invaluable work of Bernd Pfrommer for maintaining the open-source ROS drivers used for data collection and post-processing for both event and RGB cameras, as well as his valuable suggestions to generate event reconstructions. We finally would like to thank Victoria Edwards and Mariana Quesada for reviewing this manuscript.

REFERENCES

- [1] A. Q. Valenzuela and J. C. G. Reyes, “Basic spatial resolution metrics for satellite imagers,” *IEEE Sensors Journal*, vol. 19, no. 13, pp. 4914–4922, 2019.
- [2] K. Jacobsen *et al.*, “High resolution satellite imaging systems—an overview,” *Photogrammetrie Fernerkundung Geoinformation*, vol. 2005, no. 6, p. 487, 2005.
- [3] “Professional photogrammetry and drone mapping software — pix4d.com,” <https://www.pix4d.com/>, [Accessed 01-09-2024].

- [4] “Drone Mapping Software - OpenDroneMap™ — opendronemap.org,” <https://www.opendronemap.org/>, [Accessed 01-09-2024].
- [5] “Tutorials; OpenDroneMap 3.5.3 documentation — docs.opendronemap.org,” <https://docs.opendronemap.org/tutorials/>, [Accessed 01-09-2024].
- [6] X. Li, S. Cheng, Z. Zeng, C. Zhao, and C. Fan, “ERS-HDRI: Event-Based Remote Sensing HDR Imaging,” *Remote Sensing*, vol. 16, no. 3, p. 437, 2024.
- [7] N. Escudero, M. W. Hardt, and G. Inalhan, “Enabling UAVs night-time navigation through Mutual Information-based matching of event-generated images,” in *2023 IEEE/AIAA 42nd Digital Avionics Systems Conference (DASC)*. IEEE, 2023, pp. 1–10.
- [8] C. Scheerlinck, N. Barnes, and R. Mahony, “Continuous-time intensity estimation using event cameras,” in *Asian Conference on Computer Vision*. Springer, 2018, pp. 308–324.
- [9] C. Haoyu, T. Minggui, S. Boxin, W. Yizhou, and H. Tiejun, “Learning to deblur and generate high frame rate video with an event camera,” *arXiv preprint arXiv:2003.00847*, 2020.
- [10] N. Messikommer, S. Georgoulis, D. Gehrig, S. Tulyakov, J. Erbach, A. Bochicchio, Y. Li, and D. Scaramuzza, “Multi-bracket high dynamic range imaging with event cameras,” in *Proceedings of the IEEE/CVF conference on computer vision and pattern recognition*, 2022, pp. 547–557.
- [11] G. Gallego, T. Delbrück, G. Orchard, C. Bartolozzi, B. Taba, A. Censi, S. Leutenegger, A. J. Davison, J. Conradt, K. Daniilidis *et al.*, “Event-based vision: A survey,” *IEEE transactions on pattern analysis and machine intelligence*, vol. 44, no. 1, pp. 154–180, 2020.
- [12] H. Rebecq, R. Ranftl, V. Koltun, and D. Scaramuzza, “High speed and high dynamic range video with an event camera,” *IEEE transactions on pattern analysis and machine intelligence*, vol. 43, no. 6, pp. 1964–1980, 2019.
- [13] C. Brandli, L. Muller, and T. Delbrück, “Real-time, high-speed video decompression using a frame-and event-based DAVIS sensor,” in *2014 IEEE International Symposium on Circuits and Systems (ISCAS)*. IEEE, 2014, pp. 686–689.
- [14] B. Pfommer, “ssimple_image_recon - simple image reconstruction for an event based camera,” https://github.com/berndpfommer/simple-image_recon, [Accessed 06-09-2024].
- [15] A. Bisulco, F. Cladera, V. Isler, and D. D. Lee, “Fast Motion Understanding with Spatiotemporal Neural Networks and Dynamic Vision Sensors,” in *2021 IEEE International Conference on Robotics and Automation (ICRA)*, 2021, pp. 14 098–14 104.
- [16] H. Rebecq, R. Ranftl, V. Koltun, and D. Scaramuzza, “Events-to-Video: Bringing Modern Computer Vision to Event Cameras,” *IEEE Conf. Comput. Vis. Pattern Recog. (CVPR)*, 2019.
- [17] K. Chaney, F. Cladera, Z. Wang, A. Bisulco, M. A. Hsieh, C. Korpela, V. Kumar, C. J. Taylor, and K. Daniilidis, “M3ED: Multi-Robot, Multi-Sensor, Multi-Environment Event Dataset,” in *Proceedings of the IEEE/CVF Conference on Computer Vision and Pattern Recognition (CVPR) Workshops*, June 2023, pp. 4015–4022.
- [18] V. Osadciuk, M. Pudzs, A. Zujevs, A. Pecka, and A. Ardav, “Clock-based time synchronization for an event-based camera dataset acquisition platform,” in *2020 IEEE International Conference on Robotics and Automation (ICRA)*. IEEE, 2020, pp. 4695–4701.
- [19] X. Liu, G. V. Nardari, F. Cladera, Y. Tao, A. Zhou, T. Donnelly, C. Qu, S. W. Chen, R. A. F. Romero, C. J. Taylor, and V. Kumar, “Large-Scale Autonomous Flight With Real-Time Semantic SLAM Under Dense Forest Canopy,” *IEEE Robotics and Automation Letters*, vol. 7, no. 2, pp. 5512–5519, 2022.
- [20] B. Pfommer, “flir_camera_driver - ROS Teledyne FLIR camera drivers,” https://github.com/ros-drivers/flir_camera_driver/tree/humble-devel, [Accessed 16-09-2024].
- [21] J. Hurliman, “MCAP: A Next-Generation File Format for ROS Recording,” <http://download.ros.org/downloads/roscn/2022/MCAP%20A%20Next-Generation%20File%20Format%20for%20ROS%20Recording.pdf>, 2022, [Accessed 02-09-2024].
- [22] M. Folk, G. Heber, Q. Koziol, E. Pourmal, and D. Robinson, “An overview of the HDF5 technology suite and its applications,” in *Proceedings of the EDBT/ICDT 2011 workshop on array databases*, 2011, pp. 36–47.
- [23] J. Rehder, J. Nikolic, T. Schneider, T. Hinzmann, and R. Siegwart, “Extending kalibr: Calibrating the extrinsics of multiple IMUs and of individual axes,” in *2016 IEEE International Conference on Robotics and Automation (ICRA)*. IEEE, 2016, pp. 4304–4311.
- [24] G. Vivone, L. Alparone, J. Chanussot, M. Dalla Mura, A. Garzelli, G. A. Licciardi, R. Restaino, and L. Wald, “A Critical Comparison Among Pansharpening Algorithms,” *IEEE Transactions on Geoscience and Remote Sensing*, vol. 53, no. 5, pp. 2565–2586, 2015.
- [25] M. Muja and D. Lowe, “Flann-fast library for approximate nearest neighbors user manual,” *Computer Science Department, University of British Columbia, Vancouver, BC, Canada*, vol. 5, no. 6, 2009.
- [26] N. Messikommer, C. Fang, M. Gehrig, and D. Scaramuzza, “Data-driven feature tracking for event cameras,” in *Proceedings of the IEEE/CVF Conference on Computer Vision and Pattern Recognition*, 2023, pp. 5642–5651.
- [27] D. Gehrig, H. Rebecq, G. Gallego, and D. Scaramuzza, “Asynchronous, photometric feature tracking using events and frames,” in *Proceedings of the European Conference on Computer Vision (ECCV)*, 2018, pp. 750–765.
- [28] S. Guo and G. Gallego, “CMax-SLAM: Event-Based Rotational-Motion Bundle Adjustment and SLAM System Using Contrast Maximization,” *IEEE Transactions on Robotics*, vol. 40, pp. 2442–2461, 2024.